

1 **Projecting global drought risk under various SSP-RCP scenarios**

2 Zhiling Zhou¹, Liping Zhang^{1,2*}, Jie Chen¹, Dunxian She^{1,2}, Gangsheng Wang^{1,2}, Qin
3 Zhang¹, Jun Xia^{1,2}, Yanjun Zhang^{1,2}

4 ¹State Key Laboratory of Water Resources and Hydropower Engineering Science, Wu-
5 han University, Wuhan 430072, P. R. China.

6 ²Institute for Water-Carbon Cycles and Carbon Neutrality, Wuhan University, Wuhan
7 430072, P. R. China.

8 Corresponding author: Liping Zhang (zhanglp@whu.edu.cn)

9 **Key Points:**

10 (1) We present dynamic future global drought risk maps under four SSP-RCP sce-
11 narios.

12 (2) Drought risk will increase worldwide in the future, especially under SSP5-8.5.

13 (3) Among the six continents, the population and GDP under high drought risk are
14 the most in Asia and the fastest growing in Africa.

15

16 **Abstract**

17 Drought risk assessment can identify high-risk areas and bridge the gap between
18 impacts and adaptation. However, very few dynamic drought risk assessments and pro-
19 jections have been performed worldwide at high spatial resolution (e.g., $0.5^\circ \times 0.5^\circ$)
20 under different greenhouse gas emission scenarios. Here, future global drought risk is
21 projected combining three components (i.e., hazard, exposure, and vulnerability) during
22 2021–2100 under combined scenarios of Representative Concentration Pathways (RCPs)
23 and Shared Socioeconomic Pathways (SSPs): SSP1-2.6, SSP2-4.5, SSP3-7.0, and
24 SSP5-8.5. This study first investigates dynamic drought risks and exposed population and
25 GDP across the six continents (Antarctica is not examined due to data availability). The
26 results show that high-risk regions mainly concentrate in southeastern China, India,
27 Western Europe, eastern United States, and western and eastern Africa. Drought risk will
28 further strengthen in the future under four scenarios, with the highest under SSP5-8.5 and
29 the lowest under SSP3-7.0. Populations exposed to high drought risk for Asia and Africa
30 are much more than other continents. Among four SSP-RCPs, populations exposed to
31 high risk are the largest under SSP3-7.0 for Africa, Asia, and South America, while under
32 SSP5-8.5 for Australia, Europe, and North America. GDP exposed to high drought risk is
33 the largest for Asia among the six continents and the largest under SSP5-8.5 among the
34 SSP-RCPs. The most significant increases in population and GDP under high drought
35 risk both occur in Africa. This study provides a scientific basis for effective adaptation
36 measures to enhance drought resilience in potential high-risk areas.

37 **Plain Language Summary**

38 Drought increasingly affects society, economy, and ecosystems as a frequent natural
39 disaster. Drought risk assessment can help understand the extent of drought threat to the
40 human system. However, there are very few global drought risk assessments and projec-
41 tions at high spatial resolution under various climate change scenarios. Therefore, we
42 projected $0.5^\circ \times 0.5^\circ$ future drought risk during 2021-2100 under four scenarios and in-
43 vestigated exposed population and GDP across the six continents (Antarctica is not ex-
44 amined due to data availability). We find that high-risk regions mainly concentrate in
45 southeastern China, India, Western Europe, eastern United States, and western and east-
46 ern Africa. Global drought risk will increase in the future. Populations exposed to high
47 drought risk for Asia and Africa are much more than other continents. GDP exposed to

48 high drought risk is the largest for Asia among the six continents. The most significant
49 increases in population and GDP under high drought risk both occur in Africa. Our
50 findings help policymakers develop adaptive disaster prevention measures.

51 **1. Introduction**

52 Drought is one of the major severe natural disasters which leads to enormous
53 damage and costs (Lesk et al., 2016; Spinoni et al., 2014). It affects millions of people
54 each year and adversely impacts society, economy, and environment worldwide
55 (Marengo et al., 2017; Spinoni et al., 2018; Vicente-Serrano et al., 2020). The United
56 Nations Office for Disaster Risk Reduction (UNDRR) stated that people affected by
57 drought accounted for 35 percent of all natural disasters in the past two decades (ISFD
58 Reduction, 2004). Among the top ten worldwide disasters in the past 50 years (1970–
59 2019), drought was the deadliest, causing 650,000 deaths and far more economic losses
60 than other meteorological disasters (WMO, 2021). It is illustrated that drought has be-
61 come a worldwide problem and attached adverse effects to the globe.

62 In the context of global warming, the frequency and severity of droughts have in-
63 creased at the global and regional scales (Naumann et al., 2018; Takeshima et al., 2020;
64 Touma et al., 2015; Ukkola et al., 2020). Moreover, land areas affected by increasing
65 drought frequency and severity will expand under global warming with high confidence
66 as per the recently published Sixth Assessment Report of the IPCC Working Group I
67 (IPCC, 2021). Society and the economy will continuously grow simultaneously, leading
68 to more losses under droughts in the future (Su et al., 2018). Thus predicting future
69 drought risk is crucial for disaster prevention and reduction decision-making.

70 Drought risk refers to the possibility of dramatic detrimental changes due to haz-
71 ardous drought events interacting with vulnerable social conditions and ultimately re-
72 sulting in widespread adverse impacts in a community or system (IPCC, 2012). Different
73 from drought conditions, drought risk is determined not only by the intensity of drought
74 events but also by the exposure of the social-economic system and its susceptible char-
75 acteristics. Thus, drought risk is generally quantified by three primary components:
76 hazard, exposure, and vulnerability (Chou et al., 2019; Le et al., 2021; Prabnakorn et al.,
77 2019). Hazard is the physical natural drought-related characteristics. Exposure refers to
78 the presence of population and assets in places that can be affected, and vulnerability is
79 the system's feature contributing to a tendency or predisposition to adversely impacts

80 (Carrao et al., 2016; IPCC, 2012; Meza et al., 2020). Drought risk has been assessed by
81 combing hazard, exposure, and vulnerability for various regions (Guo et al., 2021; M. A.
82 A. Hoque et al., 2021; Sahana et al., 2021). In addition, pertaining to various specific
83 sectors, such as water resource, agriculture, and ecological goals, a variety of attempts
84 have been taken with different indicators of hazard, exposure, and vulnerability to assess
85 drought risk (Dai et al., 2020; X. Liu et al., 2021; Meza et al., 2020). One of the critical
86 points in drought risk assessment is the selection of indicators. Indices can be specific in
87 small regions (Khoshnazar et al., 2021; Kim et al., 2020). However, when focusing on
88 giant areas, it is a challenge to concurrently account for the comprehensiveness, accuracy,
89 and accessibility of the indicators. Population, economy, and land-use patterns were
90 generally considered (Ahmadalipour et al., 2019; Y. J. Liu & Chen, 2021). Remote
91 sensing data and GIS tools were widely applied (Palchaudhuri & Biswas, 2016; Sun et al.,
92 2014). Administrative areas were generally employed as the spatial unit during drought
93 risk assessment because socioeconomic data were customarily collected by administra-
94 tive regions (Ahmadalipour et al., 2019; Kim et al., 2020), leading to a relatively coarse
95 spatial resolution. In recent decades, the prosperous development of climate models
96 (Lehner et al., 2017; Thilakarathne & Sridhar, 2017; Y. Y. Yin et al., 2021) has provided
97 spatially accurate (e.g., below $1^\circ \times 1^\circ$ grid) projected climate data, making it possible to
98 project future drought risk with a relatively high spatial resolution. Risk predictions can
99 contribute to distinguishing the future high-risk regions and identifying the risk change
100 for specific regions.

101 Nevertheless, there are few consistent assessments and future projections across the
102 globe considering both climate change and socioeconomic developments. In addition,
103 there is a lack of predictions of populations and GDP exposed to high drought risk at
104 continental scale. In this study, we assessed global drought risk in the historical period
105 (1991–2014) and future period (2021–2100) under four climate scenarios using global
106 climate models (GCMs) in the Coupled Model Intercomparison Project Phase 6 (CMIP6).
107 The four scenarios were newly proposed in CMIP6 as a combination of Representative
108 Concentration Pathways (RCPs) and Shared Socioeconomic Pathways (SSPs): SSP1-2.6,
109 SSP2-4.5, SSP3-7.0, and SSP5-8.5 (O'Neill et al., 2016). We simultaneously considered
110 future drought changes, population and economic development, and land-use change
111 under various SSP-RCP scenarios. In addition, we Figured the exposed population and
112 GDP for six continents (Antarctica is not examined due to data availability). The aims of
113 this study are to (1) quantify the global drought risks at a $0.5^\circ \times 0.5^\circ$ resolution under four

114 SSP-RCP scenarios based on the up-to-date CMIP6 GCMs and dynamic projected so-
115 cioeconomic data; and (2) project future drought risks and associated affected population
116 and economy under high drought risk at continental scale.

117 **2. Materials and methods**

118 **2.1. Data**

119 GCMs are widely used for the projection of future climate (Cook et al., 2020;
120 Su et al., 2021; Zheng et al., 2018). Simulations including precipitation and surface
121 maximum air temperature were obtained from the GCM outputs in CMIP6. Three
122 GCMs were selected in this study based on their ability in the simulations of extre
123 me precipitation (Ayugi et al., 2021; Dong & Dong, 2021; Sian et al., 2021; Tang e
124 t al., 2021). The details of the three GCMs are shown in Table 1. The projection e
125 xperiment in CMIP6 contains a new set of emissions and land-use scenarios that co
126 mbines five SSPs and four RCPs (Riahi et al., 2017; van Vuuren et al., 2014). In t
127 his work, four combined scenarios in Tier-1 (SSP1-2.6, SSP2-4.5, SSP3-7.0, and SS
128 P5-8.5) were selected to assess the drought hazard in the future period. A bilinear i
129 nterpolation scheme was applied to interpolate the three GCMs to a common $0.5^\circ \times$
130 0.5° grid. Bias correction was conducted with the Quantile Mapping method using
131 observation data from Climate Prediction Center (CPC) in 1979–2014 as baselines.
132

133 Global 1 km population data during 2000–2014 were from WorldPop (Lloyd et al.,
134 2019). Annual population data in 1991–1999 were linearly interpolated using 1 km
135 population data in 1990, 1995, and 2000 from Global Rural-Urban Mapping Project,
136 Version 1 (Balk et al., 2006; Center for International Earth Science Information Network
137 - CIESIN - Columbia University et al., 2011). Annual GDP data with a spatial resolution
138 of 5 arc-min during 1991–2014 (Kummu et al., 2018) were used. The historical popula-
139 tion and GDP data were re-gridded to 0.5° spatial resolution. Global $0.5^\circ \times 0.5^\circ$ popula-
140 tion and GDP projections under the four SSP scenarios (Huang et al., 2019; Jiang, Wang,
141 et al., 2018; Jiang, Zhao, et al., 2018; Jing et al., 2020; Mondal et al., 2021) were em-
142 ployed for exposure and vulnerability calculations. Annual historical land cover data
143 were gained from European Space Agency (ESA) with a 300 m spatial resolution. Global
144 $0.1^\circ \times 0.1^\circ$ land cover projections from 2020 to 2100 under different RCP scenarios (Fan
145 et al., 2013, 2015; Fan, Bai, et al., 2020; Fan, Li, et al., 2020; Yue et al., 2005, 2006, 2007)

146 were utilized. Resample and zonal statistics tools in ArcGIS were used to uniform the
 147 resolution to 0.5° . The $5 \text{ min} \times 5 \text{ min}$ road density data (Meijer et al., 2018) were used
 148 and resampled to $0.5^\circ \times 0.5^\circ$. The linear density statistics tool in ArcGIS was processed to
 149 get the $0.5^\circ \times 0.5^\circ$ channel density using the river network data (Yan et al., 2019). Based
 150 on these data, the hazard, exposure, vulnerability, and risk of drought were quantified for
 151 the historical and future periods under four SSP-RCP scenarios.

152 **Table 1.**
 153 ***Information of the global climate models.***

Model	Institution	Resolution (Lon×Lat)	Calendar
EC-Earth3	EC-Earth-Consortium, Europe	$0.7^\circ \times 0.7^\circ$	gregorian
NorESM2-LM	Norwegian Climate Centre, Norway	$2.5^\circ \times 1.9^\circ$	365day
NorESM2-MM	Norwegian Climate Centre, Norway	$1.25^\circ \times 0.94^\circ$	365day

154 2.2. Quantification of drought risk

155 According to the risk definition proposed by the Intergovernmental Panel on Cli-
 156 mate Change (IPCC, 2014), drought risk is assessed through indicators of three deter-
 157 minants: hazard, exposure, and vulnerability. The risk was calculated using the formula-
 158 tion implemented by the United Nations International Strategy for Disaster Reduction
 159 (Pearson & Pelling, 2015) and IPCC (IPCC, 2012) in this study, and it has been applied in
 160 many earlier risk assessments (Ahmadalipour et al., 2019; Carrao et al., 2016; Peduzzi et
 161 al., 2009). It is defined as:

$$162 \quad \text{Risk} = \text{Hazard}^{W_H} \times \text{Exposure}^{W_E} \times \text{Vulnerability}^{W_V} \quad (1)$$

163 where W_H , W_E , W_V are the weights for hazard, exposure, and vulnerability (Table 2).

164 2.2.1 Drought hazard (DH)

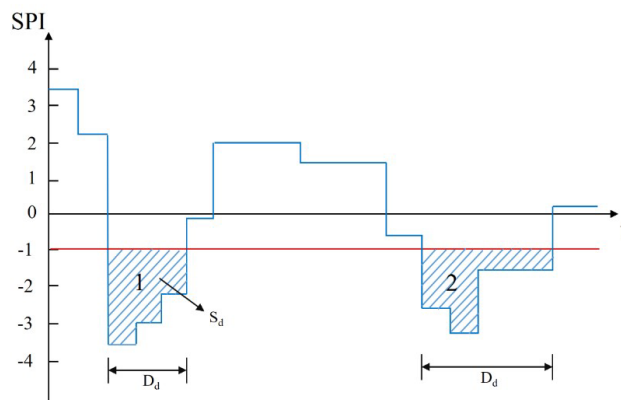
165 Hazard refers to the physical natural events that may cause disasters to human so-
 166 ciety. Standardized precipitation index (SPI; Guttman, 1999; McKee et al., 1993) was
 167 used to analyze the drought hazard in the baseline and projected periods. The SPI can
 168 quantify the lack of precipitation over multiple time scales based on the normalized
 169 probability distribution of cumulative precipitation series. It has been widely applied in
 170 drought studies because of its universality and simplicity of calculation (Dabanli et al.,
 171 2017; Dashtpagerdi et al., 2015; Kim et al., 2020). In order to identify the short-duration
 172 drought, the precipitation was cumulated every ten days, and each ten-days was fitted
 173 separately (Khoshnazar et al., 2021). Then a 3-ten-days moving average was applied to
 174 calculate the SPI.

175 Three drought characteristics were calculated from the SPI: drought severity (DS),
 176 drought frequency (DF), and drought duration (DD). Based on the run theory (Figure 1), a
 177 drought starts when the SPI value falls below the threshold and ends when the value rises
 178 above the threshold again. The threshold is -1 in this study according to McKee's classi-
 179 fication (McKee et al., 1993). Drought frequency is the number of drought events in a
 180 year. Drought duration is the number of time units (ten days in this study) between the
 181 start and the end of droughts. Drought severity is the integral of the area confined between
 182 the horizontal line below -1 and the start-end points of a drought event. If there were more
 183 than one drought in a year, we calculated the average value of DD and DS.

184 In addition to the three drought characteristics, continuous dry days (CDD) and the
 185 max temperature (TM) were also used to calculate DH. Continuous dry days are often
 186 closely associated with drought, and high temperature leads to more evaporation and
 187 contributes to drought (Cai et al., 2009). The indicator values of the three models were
 188 averaged. Thus drought hazard was calculated as:

$$189 \quad DH = DS^{W_{DS}} \times DF^{W_{DF}} \times DD^{W_{DD}} \times CDD^{W_{CDD}} \times TM^{W_{TM}} \quad (2)$$

190 where DS, DF, DD, CDD, and TM represent the drought severity, drought frequency,
 191 drought duration, continuous dry days, and the max temperature, respectively, and W_{DS} ,
 192 W_{DF} , W_{DD} , W_{CDD} , and W_{TM} are weights for DS, DF, DD, CDD, and TM, respectively.



193
 194 **Figure 1.** Schema of the run theory where D_d is the drought duration and S_d is the drought severity.

195 2.2.2 Drought exposure (DE)

196 Exposure is defined as the presence of people and economic assets in places and
 197 settings that can be adversely affected (IPCC, 2012). In this study, population and GDP
 198 were used to describe the drought exposure considering population and economy are the
 199 most directly affected by drought disasters in socioeconomic systems (Y. J. Liu & Chen,
 200 2021). Here the GDP refers to the total economic output for each grid. Drought exposure

201 was calculated as:

$$202 \quad DE = PEO^{W_{PEO}} \times GDP^{W_{GDP}} \quad (3)$$

203 where PEO and GDP represent the population (million persons) and total economic
204 output (hundred million US dollars in 2010 price) for each grid. W_{PEO} and W_{GDP} are the
205 weights for PEO and GDP, respectively.

206 **2.2.3 Drought vulnerability (DV)**

207 IPCC defined vulnerability as the property of the system's propensity to be ad-
208 versely affected (IPCC, 2012). The hybrid index-based approach was the most common
209 method used in vulnerability assessment. Despite its limitation for policy effects, com-
210 posite indicators can identify standard evaluation guidelines for impact reduction on the
211 regional to global scale (Meza et al., 2020). The United Nations International Strategy for
212 Disaster Reduction (UNISDR) proposed a drought vulnerability framework to reflect the
213 state of the social, economic, and infrastructural factors of a region (Reduction, 2004).
214 Disaster prevention and mitigation capabilities are also incorporated into vulnerability
215 considerations. These factors are mainly reflected and quantized by generic indicators
216 related to a specific exposed element (Carrao et al., 2016). In consideration of both the
217 representativeness of indicators and the availability of data, we chose four indicators: (1)
218 ratio of the cropland and built-up land in a grid (LU), reflecting the agricultural and in-
219 frastructural factors of vulnerability, (2) road density (RD), reflecting infrastructural
220 factors and transport capacity in disaster relief, (3) channel density (CD), reflecting the
221 local water resource condition, and (4) the GDP per capita (GDPP), reflecting the local
222 financial level and disaster bearing capacity. Drought vulnerability was calculated as:

$$223 \quad DV = LU^{W_{LU}} \times RD^{W_{RD}} \times CD^{W_{CD}} \times GDPP^{W_{GDPP}} \quad (4)$$

224 where W_{LU} , W_{RD} , W_{CD} , and W_{GDPP} are the weights for LU, RD, CD, and GDPP.

225 **2.3. Normalization of indicators**

226 After aggregating raw values of each indicator, a linear scale normalization (OECD,
227 2008) was performed to standardize all index values to an identical range of 0 to 1. The
228 normalization is performed by considering the maximum and minimum values of each
229 indicator among all grids. For indicators with positive (+) and negative (-) correlations to
230 drought risk (see Table 2), the normalization was calculated as:

$$\begin{cases} Z_i = \frac{X_i - X_{\min}}{X_{\max} - X_{\min}} \times 10 & \text{positive correlation} \\ Z_i = \left(1 - \frac{X_i - X_{\min}}{X_{\max} - X_{\min}}\right) \times 10 & \text{negative correlation} \end{cases} \quad (5)$$

where Z_i and X_i represent the normalized and raw indicator value for grid i , respectively, X_{\max} and X_{\min} represent the maximum and minimum values across all grids.

Finally, hazard, exposure, or vulnerability was calculated by multiplying the indicators with exponential weights:

$$Y = \prod Z_i^{W_i} \quad (6)$$

where Y is the hazard/exposure/vulnerability, and W_i is the weight for each indicator.

2.4. Weighting indicators using the Analytic Hierarchy Process

Analytical Hierarchy Process (AHP) is a flexible method to analyze complex multi-criteria decisions (Saaty & Vargas, 2001), and has been widely utilized to determine the weight of indicators in comprehensive evaluation (M. A. Hoque et al., 2020; Mokarram et al., 2021; Palchaudhuri & Biswas, 2016; Sahana et al., 2021). The weight is determined by the relative importance among the criteria through a pairwise comparison. The consistency index (CI) and the consistency ratio (CR) were used to examine the logical consistency of the weights:

$$CI = (\lambda_{\max} - n)/(n - 1) \quad (7)$$

$$CR = CI/RI \quad (8)$$

where n is the number of objects to compare, λ_{\max} is the largest eigenvalue of the pairwise comparison matrix, and RI is the randomly generated average consistency index.

More details of the AHP procedure can be found in Saaty (1987). Generally, the closer a CR is to zero, the more consistent the weights are. In this study, CR values < 0.1 were permitted. The weights were shown in Table 2.

253

254 **Table 2.**
 255 ***Drought risk assessment model.***

		Weight 1*	Indicators (correlation)	Weight 2*	Weight 1×weight 2*
Drought risk	Hazard	0.4	DS (+)	0.219	0.088
			DF (+)	0.258	0.103
			DD (+)	0.219	0.088
			CDD (+)	0.110	0.044
			TM (+)	0.194	0.078
	Exposure	0.25	POP (+)	0.5	0.125
			GDP (+)	0.5	0.125
	Vulnerability	0.35	LU (+)	0.192	0.067
			RD (-)	0.144	0.050
			CD (-)	0.349	0.122
			GDPP (-)	0.315	0.110

256 *Note.* Weight 1 is the weight of hazard, exposure, and vulnerability (equation (1)); weight 2 is the
 257 weight of each indicator in hazard, exposure, or vulnerability (equation (2), (3), (4)).

258 **3. Results**

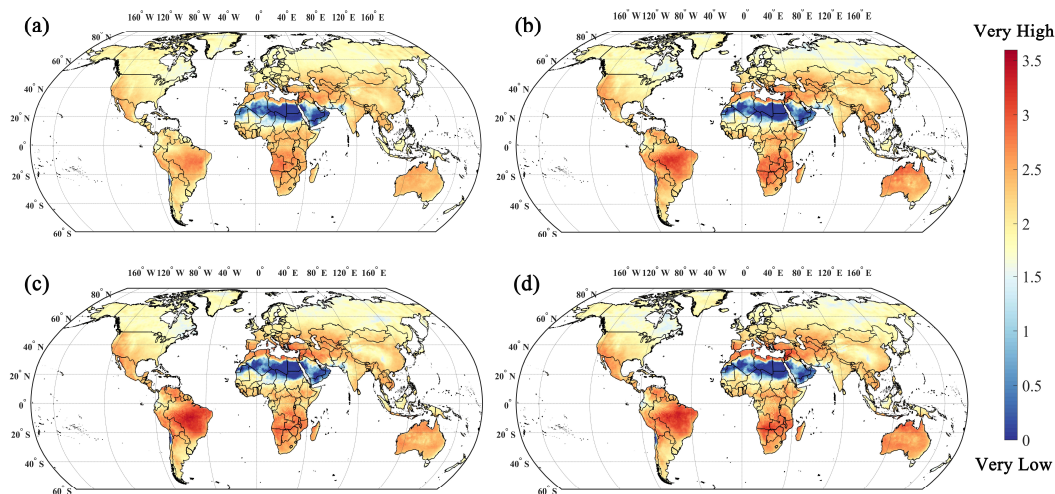
259 In this section, global drought hazard, exposure, vulnerability, and risk were calcu-
 260 lated annually in the baseline period (1991–2014) and the future period (2021–2100)
 261 under four scenarios. The global maps of the four outcomes demonstrate the average
 262 value of the historical period (1991–2014) and three future periods (near-term, 2021–
 263 2040; mid-term, 2041–2060; long-term, 2081–2100).

264 **3.1. Spatiotemporal variation in drought hazard**

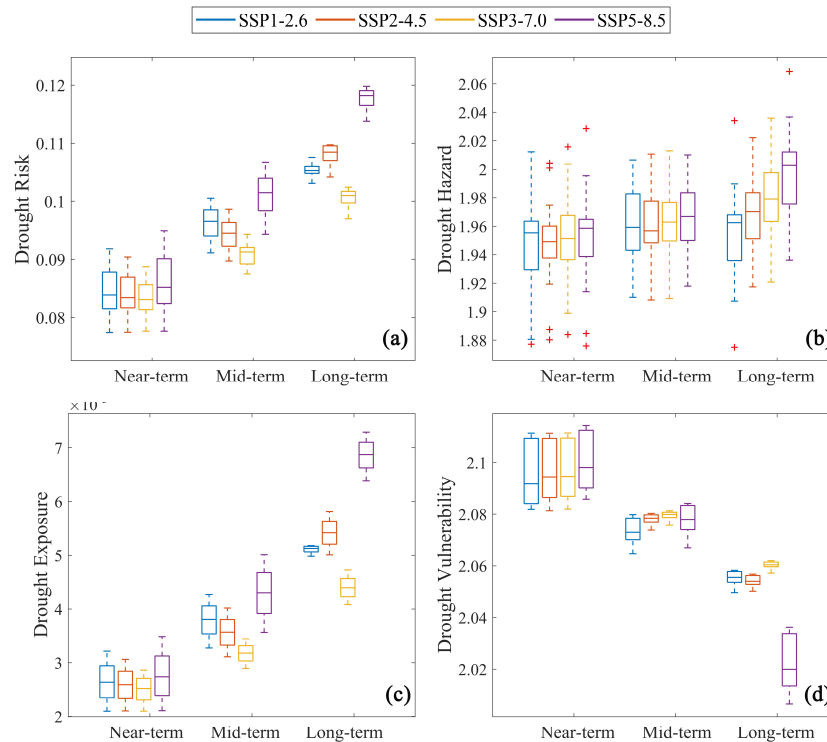
265 Figure 2 shows the global distribution of drought hazard in the baseline period and
 266 the three projected periods under SSP2-4.5 (maps under the other three scenarios are
 267 provided in Figures S1–S3 in supplementary materials). The value of drought hazard (i.e.,
 268 the product of the five normalized indicators) varies from 0 to 3.6. Generally, the spatial
 269 distribution is relatively constant, and the high levels of hazard (dark orange to red color
 270 scheme) are spatially concentrated. High drought hazard occurs in central Brazil,
 271 southwestern North America, northern and southern Africa, southern Europe, northern
 272 Middle East, and Australia. When examining the temporal change of drought hazard, it

273 appears to be more severe in the projected periods than the baseline periods. For the fu-
 274 ture period, the average global drought hazard is projected to keep increasing (Figure 3b).
 275 A transparent increasing trend can be found in high drought hazard areas (dark orange to
 276 red color scheme) while there is little change in moderate drought hazard areas (yellow
 277 color scheme) (Figure 2). The most significant change in drought hazard over time is
 278 located in central Brazil, followed by southern Africa. Hazard in high-hazard areas con-
 279 tinues to intensify from the near-term to the long-term. The difference in the high-hazard
 280 regions between the mid-term and near-term periods is more pronounced than between
 281 the long-term and mid-term periods.

282 Figure 3b compares the global average drought hazard under different scenarios for
 283 the three future periods. In the near-term, drought hazard differs slightly among the four
 284 scenarios, with median values being slightly higher under SSP1-2.6 and SSP5-8.5. In the
 285 mid-term, drought hazard is similar under the four scenarios, with median values being
 286 slightly higher under SSP3-7.0 and SSP5-8.5. In the long-term, drought hazard is more
 287 significant under high and very high (GHG) emissions (SSP3-7.0 and SSP5-8.5) than
 288 other scenarios, especially under SSP5-8.5. Among all the different scenarios and periods,
 289 drought hazard shows the most significant increase in the long-term under SSP5-8.5
 290 compared with the baseline period.



291
 292 **Figure 2.** Distribution of the global drought hazard in (a) baseline period (1991–2014) and three
 293 projected periods: (b) 2021–2040, (c) 2041–2060, and (d) 2080–2100 under SSP2-4.5. SSP, shared
 294 socioeconomic pathway.



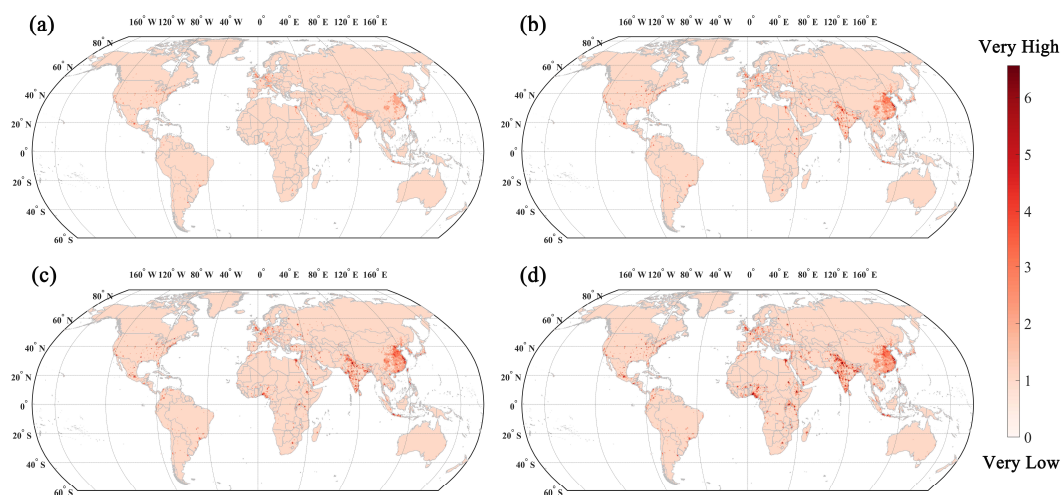
295
 296 **Figure 3.** Global drought risk (a) and its three components of drought hazard (b), drought exposure (c),
 297 and drought vulnerability (d) in the near-term (2021–2040), mid-term (2041–2060), and long-term
 298 (2081–2100) under SSP1-2.6, SSP2-4.5, SSP3-7.0, and SSP5-8.5. SSP, shared socioeconomic path-
 299 way.

300 3.2. Spatiotemporal variation in drought exposure

301 Figure 4 shows the global distribution of drought exposure in the baseline period and
 302 the three projected periods under SSP2-4.5 (maps under the other three scenarios are
 303 provided in Figures S4–S6 in supplementary materials). Generally, the spatial distribution
 304 is relatively constant, and drought exposure varies widely worldwide. High exposure
 305 concentrates in India and southeastern China, with India showing the highest value (dark
 306 red scheme). Besides, drought exposure in Western Europe also maintains a relatively
 307 high level, especially in southern England, northern France, Netherlands, and north-
 308 western Germany. So do the east and west coasts and state capitals in the United States.
 309 The worsening high exposure emerges in Africa, especially in southern Nigeria, northern
 310 Egypt, and central Ethiopia. Temporally, drought exposure gets significantly higher in the
 311 projected periods than the baseline period, especially in the high-exposed areas. Global
 312 average drought exposure shows an increasing trend over time under all scenarios (Figure
 313 3c). In the near-term and mid-term, the increase is more significant in India and south-

314 eastern China compared to other regions. In the long-term, however, the greater increase
 315 is located in western and eastern Africa and India. Drought exposure in North America
 316 and Western Europe increases less pronouncedly.

317 Figure 3c compares the global average drought exposure under different scenarios in
 318 the three future periods. The differences among different scenarios are projected to get
 319 larger over time. Among the four SSPs, drought exposure is the highest under SSP5-8.5
 320 and the lowest under SSP3-7.0 in all three future periods. Exposure under SSP1-2.6 is
 321 higher than that under SSP2-4.5 in the near-term and mid-term, while turning opposite in
 322 the long-term. The interquartile range of drought exposure values is minimal under
 323 SSP1-2.6 in the long-term.



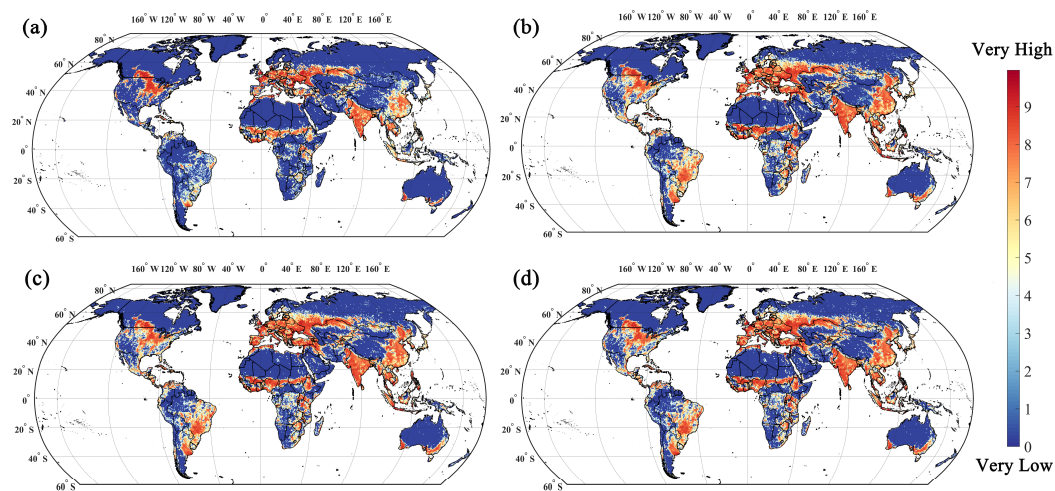
324 **Figure 4.** Distribution of the global drought exposure in (a) baseline period (1991–2014) and three
 325 projected periods: (b) 2021–2040, (c) 2041–2060, and (d) 2080–2100 under SSP2-4.5. SSP, shared
 326 socioeconomic pathway.
 327

328 3.3. Spatiotemporal variation in drought vulnerability

329 Figure 5 shows the spatial distribution of drought vulnerability in the baseline period
 330 and the three projected periods under SSP2-4.5 (maps under the other three scenarios are
 331 provided in Figures S7–S9 in supplementary materials). The distributions are similar
 332 among different periods and scenarios with high vulnerability occurring in the regions
 333 covered with cropland and building land. High vulnerable regions and countries are
 334 eastern China, India, Southeastern Asia, Europe below 60°N latitude, western and eastern
 335 Africa, southern Australia, central and western United States, southern Mexico, and
 336 southeastern South America. Temporally, drought vulnerability in the projected periods is
 337 higher than in the baseline period, especially in the eastern United States, southern Brazil,

338 eastern Argentina, southern Africa, and eastern China. Global average drought vulnera-
 339 bility shows a decreasing trend over time in the future under all scenarios (Figure 3d).

340 Figure 3d demonstrates the differences in drought vulnerability under various SSPs
 341 in the three future periods. Among the four scenarios, the decrease of drought vulnera-
 342 bility across time under SSP5-8.5 is projected to be the largest. In the near-term and
 343 mid-term, drought vulnerability is similar under the four SSPs, while significantly
 344 smaller under SSP5-8.5 than the other three scenarios in the long-term. In the mid-term
 345 and long-term, the interquartile ranges of drought vulnerability value are minimal under
 346 SSP2-4.5 and SSP3-7.0.



347 **Figure 5.** Distribution of the global drought vulnerability in (a) baseline period (1991–2014) and three
 348 projected periods: (b) 2021–2040, (c) 2041–2060, and (d) 2080–2100 under SSP2-4.5. SSP, shared
 349 socioeconomic pathway.
 350

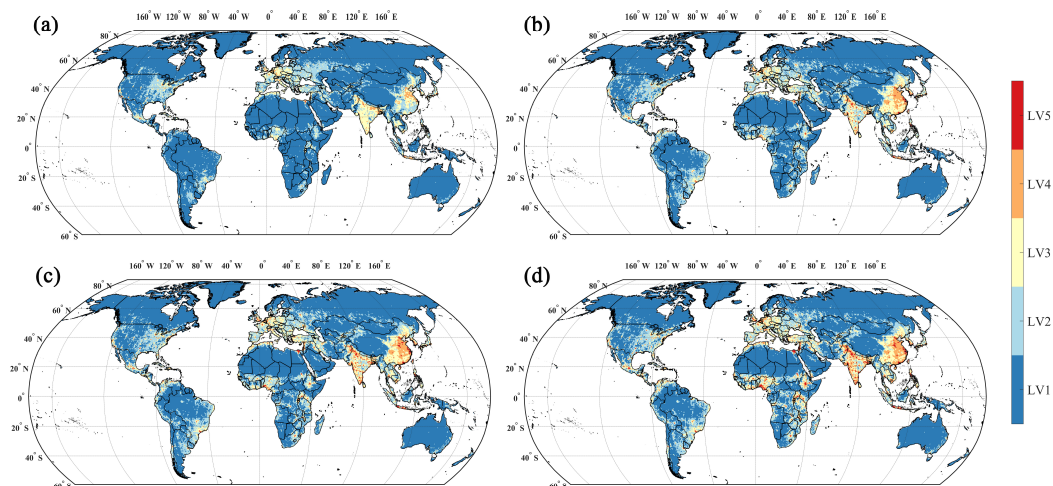
351 3.4. Future drought risk projection

352 3.4.1. Global drought risk map

353 Drought risk maps under SSP2-4.5 are shown in Figure 6 (maps under the other
 354 three scenarios are presented in Figures S10–S12 in supplementary materials). The raw
 355 risk values were classified into five grades using the natural breaks method (Basofi et al.,
 356 2015). The spatial distributions of drought risk are similar under the various scenarios and
 357 periods. The regions with high drought risk are concentrated in socially and economically
 358 developed areas. Sparsely populated regions demonstrated lower drought risk levels. The
 359 specific high-risk areas are (1) Africa: the Nile Delta from Cairo to Tanta in northern
 360 Egypt, Khartoum and its surrounding southern areas in Sudan, Addis Ababa and its sur-

361 rounding areas in Ethiopia, Uganda, southern Kenya, southern Cote d'Ivoire, northern
 362 Morocco and Algeria, and the capital city of South Africa, Zambia, Congo; (2) Asia:
 363 southeastern China, especially the Pearl River Delta, Yangtze River delta, and the North
 364 China Plain; northern and southwestern India, northern Pakistan, western Syria, eastern
 365 Iraq, Manila in the Philippines, and Jakarta; (3) Austria: almost none region above level 4
 366 with risk in the southeastern part relatively higher; (4) Europe: southern England, Neth-
 367 erlands, and big cities such as Paris, Berlin, Moscow, and their surrounding areas; (5)
 368 North America: southern Mexico and the eastern United States; and (6) South America:
 369 northern Colombia, northern Venezuela, and southern Brazil. The highest concentrations
 370 of high risk are in India and eastern China. In terms of temporal change, drought risk gets
 371 higher in the projected periods than the baseline period and keeps increasing in the future
 372 (Figure 3a). However, the rapid growth period differs spatially over the globe. From the
 373 near-term to the mid-term, drought risk increases faster in southeastern China, India,
 374 northern Egypt. From the mid-term to the long-term, drought risk increases faster in
 375 western and eastern Africa.

376 Figure 3a demonstrates the differences in drought risk under various SSPs in the
 377 three future periods. Among the four scenarios, drought risk is the highest under
 378 SSP5-8.5 in all the three future periods, followed by SSP1-2.6 and SSP2-4.5, and drought
 379 risk under SSP3-7.0 is the lowest. In addition, the differences in drought risk under dif-
 380 ferent SSPs enlarger across time. The interquartile range of risk values in each period
 381 decreases from the near-term to the long-term.



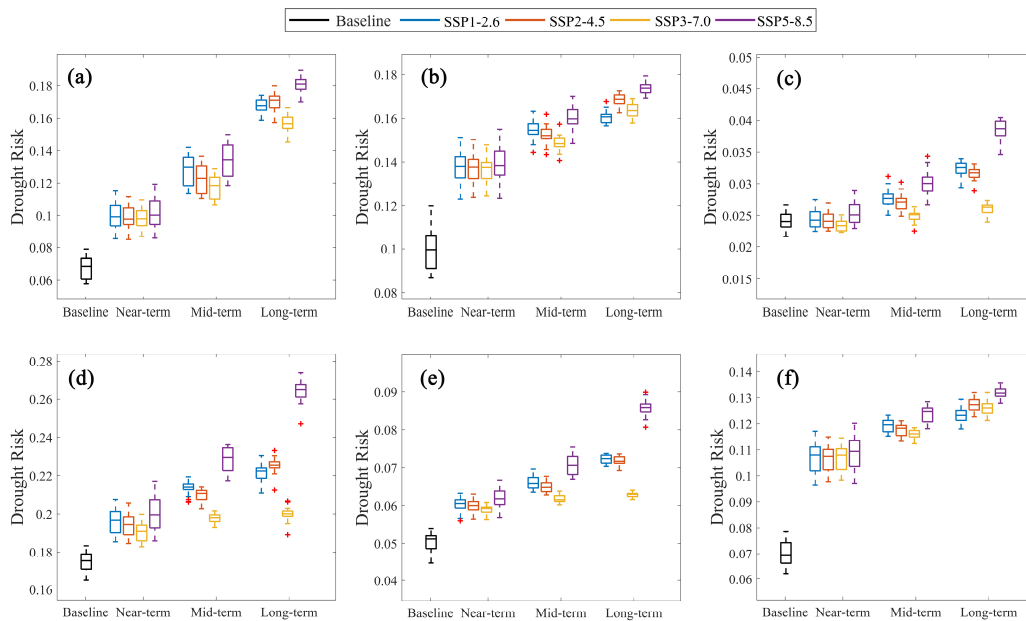
382
 383 **Figure 6.** Distribution of the global drought risk in (a) baseline period (1991–2014) and three pro-
 384 jected periods: (b) 2021–2040, (c) 2041–2060, and (d) 2080–2100 under SSP2-4.5. SSP, shared so-
 385 cioeconomic pathway; LV, level.

386 3.4.2. Continental drought risk projections

387 Figure 7 presents the temporal change of the spatial average drought risk under four
388 SSPs for the six continents (excluding Antarctica). Drought risks for all six continents are
389 projected to increase under the four scenarios. The highest average drought risk is ob-
390 served in Europe, followed by Africa and Asia among the six continents. South America
391 and North America rank fourth and fifth, respectively, and risk in Australia is the lowest.
392 Africa has the most significant increase in drought risk, with the long-term period being
393 almost three times greater than the baseline period under SSP5-8.5. From the baseline to
394 the long-term period, the growth rates are about 60%, 60%, 45%, 70%, and 85% for Asia,
395 Australia, Europe, North America, and South America under SSP5-8.5, respectively.
396 Drought risk for Asia and South America increases more significantly from the baseline
397 to the near-term period than from the near-term to the long-term period. In contrast, an
398 opposite pattern is observed for Australia. The increase rates for other continents are
399 relatively stable. Among the four SSPs, drought risk under SSP5-8.5 is the highest for all
400 continents, while SSP3-7.0 is the lowest, and the difference between the two scenarios
401 enlarges over time. Differences in drought risk between the four scenarios are significant
402 in Australia, Europe, and North America, while much smaller in Africa, Asia, and South
403 America. Drought risk under SSP1-2.6 is slightly higher than under SSP2-4.5 in the
404 near-term, and the difference enlarges in the mid-term for all continents. In the long-term,
405 drought risk under SSP2-4.5 turns out to be higher than SSP1-2.6 for Africa, Asia, Europe,
406 and South America, while still lower than under SSP1-2.6 in Australia and North Amer-
407 ica.

408 Figure 8 shows the proportions of high drought risk grids (Level 4 and 5) for the six
409 continents. The temporal changes are similar to the changes in the average drought risk
410 (Figure 7) for all the continents under the four scenarios. Generally, the proportions of
411 high-risk grids are more in Europe, Asia, and Africa. In the long-term, the upper quartile
412 of proportion for Europe exceeds 10% under SSP5-8.5, with about 6% under SSP1-2.6
413 and SSP2-4.5 and 4% under SSP3-7.0. For Asia, the proportions under the four scenarios
414 are relatively similar. The medians increase from 2% in the baseline period to about 5% in
415 the near-term. Medians are 6% to 7% in the mid-term and 7% to 8% in the long-term. For
416 Africa, the proportions of high-risk grids increase from 0.2% in the baseline period to
417 around 5% in the long-term. The medians of high-risk proportion for North America and
418 South America are close, and the highest values are about 2.2% in the long-term under

419 SSP5-8.5. High-risk grids proportions for Australia are the least, and the upper quartiles
 420 are always lower than 1% in all periods. Similar to the spatially average risk, the high-risk
 421 proportion under SSP5-8.5 is the highest among the four SSPs for all continents, while
 422 SSP3-7.0 is the lowest. The difference between the four scenarios increases over time,
 423 especially in Australia, Europe, and North America. The proportions under SSP1-2.6 and
 424 SSP2-4.5 are close for all six continents in the near-term. However, in the mid-term, the
 425 high-risk proportion under SSP1-2.6 is higher than that under SSP2-4.5, especially for
 426 Africa and South America. On the contrary, the high-risk proportion under SSP2-4.5 is
 427 higher than SSP1-2.6 in the long-term for all continents except Australia.



428
 429 **Figure 7.** Spatial drought risk of (a) Africa, (b) Asia, (c) Australia, (d) Europe, (e) North America, and
 430 (f) South America in the baseline period (1991–2014), near-term (2021–2040), mid-term (2041–2060),
 431 and long-term (2080–2100) under SSP1-2.6, SSP2-4.5, SSP3-7.0, and SSP5-8.5. SSP, shared socio-
 432 economic pathway.

433
434 **Figure 8.** The proportion of grids with drought risk above Level 3 for (a) Africa, (b) Asia, (c) Australia,
435 (d) Europe, (e) North America, and (f) South America in the baseline period (1991-2014), near-term
436 (2021–2040), mid-term (2041–2060), and long-term (2080–2100) under SSP1-2.6, SSP2-4.5,
437 SSP3-7.0, and SSP5-8.5. SSP, shared socioeconomic pathway.

438 **3.4.3. Continental population and GDP under high drought risk**

439 We counted the population and GDP at high drought risk (above Level 3, Figure 9
440 and Figure 10) and the highest drought risk (Level 5, Figure S13 and Figure S14 in sup-
441plementary materials) for the six continents in the baseline period and three projected
442 periods under four SSPs. Figure 9 shows that the total populations under high and the
443 highest drought risk both increase in the projected periods than the baseline period for all
444 the six continents. Among the six continents, populations under high and the highest risk
445 for Asia are both the largest, with the maximum values reaching 5 billion and almost 3
446 billion in the long-term under SSP3-7.0. Africa is the second largest with the medians of
447 more than 2 and 1.3 billion under high and the highest risk in the long-term under
448 SSP3-7.0. In addition, Africa has the most significant increase in population under high
449 and the highest risk. The total populations under high and the highest drought risk for
450 Europe and North America are close, reaching about 600 and over 300 billion in the
451 long-term under SSP5-8.5. Comparing the four scenarios, the total populations under
452 high risk are similar in the near-term. However, the differences among the different SSPs
453 enlarge in the mid-term and long-term. For Africa, Asia, and South America, the total
454 population under high risk is the largest under SSP3-7.0, followed by SSP2-4.5, and

455 similar under the other two SSPs. For Australia, Europe, and North America, the total
456 population under high risk is the largest under SSP5-8.5 with the lowest under SSP3-7.0,
457 and the values are similar under SSP1-2.6 and SSP2-4.5. Under the highest risk, the rel-
458 ative population size among the four scenarios is consistent with the high risk for all six
459 continents.

460 Figure 10 shows the total GDPs under high and the highest drought risk keep in-
461 creasing for all continents. Similar to the population, the most significant increases in
462 GDP under high and the highest risk both occur in Africa, with the median of the total
463 GDP under high drought risk reaching 100 trillion US dollars (2010 price) under
464 SSP5-8.5 in the long-term. The values under the highest risk are about 2/3 as high risk.
465 The total GDPs under high and the highest drought risk are both the largest for Asia, with
466 the median over 350 and 200 trillion, respectively. GDPs under high drought risk for
467 Europe and North America are close, and Australia is the smallest. Comparing the four
468 scenarios, the total GDPs under high risk are similar in the near-term, and the differences
469 among the different SSPs enlarge in the mid-term and long-term. The total GDP exposed
470 to high risk is the largest under SSP5-8.5 and the smallest under SSP3-7.0 for all conti-
471 nents. The values are similar under SSP1-2.6 and SSP2-4.5. The differences between the
472 SSP5-8.5 and other SSPs are significant for Australia, Europe, and North America. Under
473 the highest risk, the relative GDP size among the four scenarios is consistent with the high
474 risk for all six continents.

475

476 **Figure 9.** The total population under drought risk above Level 3 for (a) Africa, (b) Asia, (c) Australia,

477 (d) Europe, (e) North America, and (f) South America in the baseline period (1991-2014), near-term
478 (2021–2040), mid-term (2041–2060), and long-term (2080–2100) under SSP1-2.6, SSP2-4.5,
479 SSP3-7.0, and SSP5-8.5. SSP, shared socioeconomic pathway.

480
481 **Figure 10.** The total GDP under drought risk above Level 3 for (a) Africa, (b) Asia, (c) Australia, (d)
482 Europe, (e) North America, and (f) South America in the baseline period (1991-2014), near-term
483 (2021–2040), mid-term (2041–2060), and long-term (2080–2100) under SSP1-2.6, SSP2-4.5,
484 SSP3-7.0, and SSP5-8.5. GDP, Gross Domestic Product; SSP, shared socioeconomic pathway.

485 **4. Discussion**

486 This study presents the future global drought risk map under SSP1-2.6, SSP2-4.5,
487 SSP3-7.0, and SSP5-8.5, combining hazard, exposure, and vulnerability. Drought risk for
488 the six continents and their population and GDP under high drought risk is specifically
489 analyzed. The results show that high drought hazard areas are mainly distributed in cen-
490 tral Brazil, southwestern North America, northern and southern Africa, southern Europe,
491 southwestern Asia, and Australia, which is generally consistent with the drought-prone
492 areas in the previous studies (Carrao et al., 2016; Li et al., 2021; Lu et al., 2019). However,
493 drought hazard in central Brazil and North America is higher herein than in some pre-
494 vious studies (Carrao et al., 2016; Wang et al., 2021). Such differences may arise from the
495 selection of drought indexes and meteorological data from different sources. We used
496 3-ten-days SPI to identify drought, and thus more short droughts were identified. When
497 examining the temporal change, the global average drought hazard shows an increasing

498 trend in the future, especially under SSP5-8.5, which is similar to the previous findings
499 (Li et al., 2021).

500 In the exposure analysis, drought exposure is significantly higher in the developed
501 areas and increases significantly in the future. Among the four SSPs, drought exposure is
502 the highest under SSP5-8.5 and the lowest under SSP3-7.0. In addition, we found that
503 exposure values under SSP1-2.6 in the long-term are concentrated, implying that drought
504 exposure may reach a peak and stop growing after 2080 under SSP1-2.6. Vulnerability
505 assessment is complicated since it reflects the adaptation and sensitivity levels of the social
506 system to drought. In this study, ratios of the cropland and built-up land, road density, and
507 channel density were chosen to reflect the agricultural and infrastructure factors and
508 water resource conditions. In addition, we used the GDP per capita to represent the re-
509 sistance to drought disasters. The high vulnerable regions are observed in eastern China,
510 India, Southeastern Asia, Western Europe, western and eastern Africa, southern Australia,
511 central and western United States, southern Mexico, and southeastern South America.
512 These are places where cultivated land and human settlements are concentrated. The
513 distribution is similar to previous studies (Carrao et al., 2016; Y. J. Liu & Chen, 2021),
514 while several differences exist due to the selection of indicators. Global average drought
515 vulnerability shows a decreasing trend over time in the future since the GDP per capita
516 increases significantly. In the mid-term and long-term, the interquartile range of drought
517 vulnerability values are very small under SSP2-4.5 and SSP3-7.0, showing that drought
518 vulnerability may stop decreasing and maintain stability after 2040 under these two
519 scenarios.

520 As revealed in this study, the high drought risk regions are mainly distributed in the
521 areas with high exposure, which is consistent with the previous studies (Carrao et al.,
522 2016; Y. J. Liu & Chen, 2021). In the future, consistent with other studies (Ahmadalipour
523 et al., 2019; Song et al., 2021; Q. Zhang et al., 2019), average drought risk and high risk
524 are projected to keep increasing. Among the four SSPs, drought risk is the highest under
525 SSP5-8.5, followed by SSP1-2.6, SSP2-4.5, and SSP3-7.0, while in some studies the
526 order may be different due to the different combinations of the SSPs and RCPs. However,
527 it is consistent that the drought risk is higher under the scenarios with high greenhouse
528 gas emissions and more population and GDP (Ahmadalipour et al., 2019; Y. J. Liu &
529 Chen, 2021). In addition, the interquartile range of risk values in each period decreases
530 from the near-term to the long-term, showing that the growth rate of drought risk de-
531 creases over time, which is consistent with other findings (Ahmadalipour et al., 2019;

532 Mondal et al., 2021).

533 To better understand the drought risk for the continents, we counted the drought risk
534 at continental scale. Among the six continents, the highest average drought risk and ratios
535 of high drought risk grids are in Europe, followed by Asia and Africa, resulting from the
536 high proportions of urbanization and cropland. Risk is the highest under SSP5-8.5 and
537 lowest under SSP3-7.0 for all continents, and the difference is more significant for Eu-
538 rope, North America, and Australia. That is because population and GDP vary more
539 largely under different SSPs for the three developed continents in the long-term than the
540 less developed continents. The population and GDP under high risk for each continent
541 remind that more attention should be paid to countries in Asia and Africa because of their
542 vast amount and rapid increases in the social economy. Among the four SSPs, the popu-
543 lation under high risk for the less developed continents (Africa, Asia, and South America)
544 is the largest under SSP3-7.0, with being the lowest under this scenario for the other three
545 continents. The reason is that the SSP3-7.0 is a scenario of an imbalanced developed and
546 regionally differentiated world, with faster population growth in developing countries,
547 constrained by educational and technological development. The population under high
548 risk for the relatively well-developed continents (Europe, North America, and South
549 America) is the largest under SSP5-8.5 among different SSP, likely due to the population
550 migration to socioeconomically developed areas. For GDP, differences between the
551 SSP5-8.5 and other SSPs are more significant for Australia, Europe, and North America.
552 These differences among the developed and less developed continents may result from
553 spatial development inequality under different SSPs. The largest increases in population
554 and GDP under high drought risk both occur in Africa, reminding that effective drought
555 hazard adaptation measures are in urgent need to be taken to enable socioeconomic sys-
556 tems in Africa.

557 There are some limitations in this study due to uncertainties during the assessment
558 process, including the uncertainties in the choice of indicators and uncertainties in the
559 indicator data. On the one hand, the indicators can be more diverse and comprehensive
560 when the data are available. In hazard analysis, other drought indices such as the Palmer
561 drought severity index (Palmer, 1965) and the standardized precipitation evapotranspi-
562 ration index (Vicente-Serrano et al., 2010) can also be used. In exposure and vulnerability
563 assessment, other socioeconomic factors that influence exposure and vulnerability, such
564 as the age/sex structure and the industrial structure should also be considered. In addition,
565 the density and volume of the reservoirs should be taken into account as the drought

566 disaster reduction ability. Different indicators may result in inconsistent results (Yao et al.,
567 2018; X. Zhang et al., 2017). On the other hand, there are uncertainties in selecting GCMs
568 and projections of population, GDP, and land use. Climate models are also subject to
569 significant uncertainty (Monerie et al., 2020; Tabari et al., 2019). Nevertheless, in this
570 study, bias corrections have been conducted to improve the GCMs outputs, and the pro-
571 jections of socioeconomic data were simulated under different SSP scenarios. In addition,
572 uncertainty exists in all studies on future projections that cannot be avoided entirely (Q.
573 Yin et al., 2019). Therefore, the results of this study can be considered to be reasonable. In
574 further studies, more comprehensive assessment models can be used to predict drought
575 risk by combining more accurate available data with higher resolution.

576 **5. Conclusion**

577 We assessed and predicted global drought risk under various SSP-RCP scenarios by
578 adopting the risk quantification formula proposed by IPCC and selecting evaluation in-
579 dicators of hazard, exposure, and vulnerability. Three key findings are summarized as
580 follows.

581 (1) High drought risk areas are mainly distributed in southeastern China, India,
582 Western Europe, eastern United States, and western and eastern Africa. Global drought
583 risk gets higher in the projected periods than the baseline period and keeps increasing in
584 the future. Among the four SSPs, the highest and lowest drought risk would be under
585 SSP5-8.5 and SSP3-7.0, respectively.

586 (2) Averaged drought risk and high risk for all six continents are projected to in-
587 crease under the four scenarios. Europe, Asia, and Africa are projected to be the conti-
588 nents with higher average risk and more high-risk grids among the six continents. Among
589 the four SSPs, drought risk under SSP5-8.5 is the highest for all continents, while
590 SSP3-7.0 is the lowest.

591 (3) Populations under high drought risk for Asia and Africa are much more massive
592 than other continents, with being the most for Asia. For Africa, Asia, and South America,
593 the total populations exposed to high risk are the largest under SSP3-7.0, followed by
594 SSP2-4.5 and similar under SSP1-2.6 and SSP5-8.5. For Australia, Europe, and North
595 America, the total populations exposed to high risk are the largest under SSP5-8.5 with
596 the smallest under SSP3-7.0, and the values are similar under SSP1-2.6 and SSP2-4.5.
597 GDP under high drought risk in Asia is the highest among the six continents. Among the

598 four scenarios, the total GDP under high risk is the largest under SSP5-8.5 and the
599 smallest under SSP3-7.0 for all continents, with being similar under SSP1-2.6 and
600 SSP2-4.5. The most significant increases in population and GDP under high drought risk
601 both occur in Africa.

602 Overall, the findings of this study highlight the relative sensitivity of socioeconomic
603 drought risk to different SSP-RCP scenarios across the globe. Our research can be a
604 bridge between physical and social sciences to help policymakers develop effective
605 adaptive techniques to enhance drought resilience.

606 **Acknowledgments**

607 This work is supported by the National Key Research and Development Program of
608 China (No.2017YFA0603704). We also acknowledge support by Major projects of the
609 National Natural Science Foundation of China (No.41890824) and the Excellent Young
610 Scientists Fund, and the Strategic Priority Research Program of the Chinese Academy of
611 Sciences (No. XDA23040500).

612 **Author contributions**

613 LPZ conceived the original idea, and ZLZ designed the methodology. LPZ, JC, and
614 YJZ collected the data. ZLZ developed the code and performed the analysis, with some
615 contributions from QZ and DXS. ZLZ, LPZ, JC, and DXS contributed to the interpreta-
616 tion of results. ZLZ wrote the first version of the manuscript, and LPZ, JC, GSW, and JX
617 revised the paper.

618 **Data availability**

619 The climate simulation data can be accessed from the CMIP6 archive
620 (<https://esgf-node.llnl.gov/projects/cmip6/>). The observation climate data during can be
621 accessed from National Oceanic and Atmospheric Administration (NOAA) Physical
622 Sciences Laboratory (<https://psl.noaa.gov/data/gridded/index.html>). Global annual 1 km
623 population data during 2000 to 2014 can be accessed from WorldPop archive
624 (<https://www.worldpop.org/geodata/listing?id=64>). Global 1 km population data in 1990,
625 1995, and 2000 can be accessed from Socioeconomic Data and Applications Center
626 (SEDAC) (<https://sedac.ciesin.columbia.edu/data/collection/grump-v1>). Global annual 5

627 arc-min GDP data during 1991 to 2014 can be accessed from Dryad Data
628 (<https://datadryad.org/stash/dataset/doi:10.5061/dryad.dk1j0>). Projected 0.5° gridded
629 global population and GDP data can be accessed from figshare
630 (<https://figshare.com/s/5433bdfcb503fbac8303>). Global annual 300m land cover data
631 during 1991 to 2014 can be gained from European Space Agency (ESA,
632 <https://www.esa-landcover-cci.org/?q=node/197>). Global 0.1° × 0.1° land cover projec-
633 tions can be gained from figshare (<https://figshare.com/s/ace7581c0863241ac5e1>).
634 Global road density data can be accessed from the Global Roads Inventory Project (GRIP)
635 dataset (<https://www.globio.info/download-grip-dataset>). Global river network data can
636 be gained from figshare
637 ([https://figshare.com/articles/dataset/A_data_set_of_global_river_networks_and_corres
638 ponding_water_resources_zones_divisions/8044184/6](https://figshare.com/articles/dataset/A_data_set_of_global_river_networks_and_corres_ponding_water_resources_zones_divisions/8044184/6)).

639 **Conflict of interest**

640 The authors declare that they have no conflict of interest with the work presented
641 here.

642 **References**

- 643 Ahmadalipour, A., Moradkhani, H., Castelletti, A., & Magliocca, N. (2019). Future
644 drought risk in Africa: Integrating vulnerability, climate change, and population
645 growth. *Science of the Total Environment*, 662, 672–686.
646 <https://doi.org/10.1016/j.scitotenv.2019.01.278>
- 647 Ayugi, B., Zhihong, J., Zhu, H. H., Ngoma, H., Babaousmail, H., Rizwan, K., & Dike, V.
648 (2021). Comparison of CMIP6 and CMIP5 models in simulating mean and extreme
649 precipitation over East Africa. *International Journal of Climatology*, 41(15), 6474–
650 6496. <https://doi.org/10.1002/joc.7207>
- 651 Balk, D. L., Deichmann, U., Yetman, G., Pozzi, F., Hay, S. I., & Nelson, A. (2006).
652 Determining Global Population Distribution: Methods, Applications and Data.
653 *Advances in Parasitology*, 62, 119–156. Retrieved from
654 [https://doi.org/10.1016/S0065-308X\(05\)62004-0](https://doi.org/10.1016/S0065-308X(05)62004-0)
- 655 Cai, W. J., Cowan, T., Briggs, P., & Raupach, M. (2009). Rising temperature depletes soil
656 moisture and exacerbates severe drought conditions across southeast Australia.
657 *Geophysical Research Letters*, 36. <https://doi.org/10.1029/2009gl040334>

- 658 Carrao, H., Naumann, G., & Barbosa, P. (2016). Mapping global patterns of drought risk:
659 An empirical framework based on sub-national estimates of hazard, exposure and
660 vulnerability. *Global Environmental Change-Human and Policy Dimensions*, 39,
661 108–124. <https://doi.org/10.1016/j.gloenvcha.2016.04.012>
- 662 Center for International Earth Science Information Network - CIESIN - Columbia
663 University, International Food Policy Research Institute - IFPRI, The World Bank,
664 & Centro Internacional de Agricultura Tropical - CIAT. (2011). Global Rural-Urban
665 Mapping Project, Version 1 (GRUMPv1) [Dataset]: Population Count Grid.
666 Palisades, NY: NASA Socioeconomic Data and Applications Center (SEDAC).
667 <https://doi.org/10.7927/H4VT1Q1H>
- 668 Chou, J. M., Xian, T., Zhao, R. Z., Xu, Y., Yang, F., & Sun, M. Y. (2019). Drought Risk
669 Assessment and Estimation in Vulnerable Eco-Regions of China: Under the
670 Background of Climate Change. *Sustainability*, 11(16).
671 <https://doi.org/10.3390/su11164463>
- 672 Cook, B. I., Mankin, J. S., Marvel, K., Williams, A. P., Smerdon, J. E., & Anchukaitis, K.
673 J. (2020). Twenty-First Century Drought Projections in the CMIP6 Forcing
674 Scenarios. *Earths Future*, 8(6). <https://doi.org/10.1029/2019ef001461>
- 675 Dabanli, I., Mishra, A. K., & Sen, Z. (2017). Long-term spatio-temporal drought
676 variability in Turkey. *Journal of Hydrology*, 552, 779–792.
677 <https://doi.org/10.1016/j.jhydrol.2017.07.038>
- 678 Dai, M., Huang, S. Z., Huang, Q., Leng, G. Y., Guo, Y., Wang, L., et al. (2020).
679 Assessing agricultural drought risk and its dynamic evolution characteristics.
680 *Agricultural Water Management*, 231. <https://doi.org/10.1016/j.agwat.2020.106003>
- 681 Dashtpaderdi, M. M., Kousari, M. R., Vagharfard, H., Ghonchepour, D., Hosseini, M. E.,
682 & Ahani, H. (2015). An investigation of drought magnitude trend during 1975-2005
683 in arid and semi-arid regions of Iran. *Environmental Earth Sciences*, 73(3), 1231–
684 1244. <https://doi.org/10.1007/s12665-014-3477-1>
- 685 Dong, T. Y., & Dong, W. J. (2021). Evaluation of extreme precipitation over Asia in
686 CMIP6 models. *Climate Dynamics*, 57(7–8), 1751–1769.
687 <https://doi.org/10.1007/s00382-021-05773-1>
- 688 Fan, Z. M., Li, J., & Yue, T. X. (2013). Land-cover changes of biome transition zones in
689 Loess Plateau of China. *Ecological Modelling*, 252, 129–140.
690 <https://doi.org/10.1016/j.ecolmodel.2012.07.039>
- 691 Fan, Z. M., Li, J., Yue, T. X., Zhou, X., & Lan, A. J. (2015). Scenarios of land cover in

- 692 Karst area of Southwestern China. *Environmental Earth Sciences*, 74(8), 6407–6420.
693 <https://doi.org/10.1007/s12665-015-4223-z>
- 694 Fan, Z. M., Li, S. B., & Fang, H. Y. (2020). Explicitly Identifying the Desertification
695 Change in CMREC Area Based on Multisource Remote Data. *Remote Sensing*,
696 12(19). <https://doi.org/10.3390/rs12193170>
- 697 Fan, Z. M., Bai, R. Y., & Yue, T. X. (2020). Scenarios of land cover in Eurasia under
698 climate change. *Journal of Geographical Sciences*, 30(1), 3–17.
699 <https://doi.org/10.1007/s11442-020-1711-1>
- 700 Guo, H., Wang, R., Garfin, G. M., Zhang, A. Y., Lin, D. G., Liang, Q. O., & Wang, J. A.
701 (2021). Rice drought risk assessment under climate change: Based on physical
702 vulnerability a quantitative assessment method. *Science of the Total Environment*,
703 751. <https://doi.org/10.1016/j.scitotenv.2020.141481>
- 704 Guttman, N. B. (1999). Accepting the standardized precipitation index: A calculation
705 algorithm. *Journal of the American Water Resources Association*, 35(2), 311–322.
706 <https://doi.org/10.1111/j.1752-1688.1999.tb03592.x>
- 707 Hoque, M. A., Pradhan, B., & Ahmed, N. (2020). Assessing drought vulnerability using
708 geospatial techniques in northwestern part of Bangladesh. *Science of the Total*
709 *Environment*, 705. <https://doi.org/10.1016/j.scitotenv.2019.135957>
- 710 Hoque, M. A. A., Pradhan, B., Ahmed, N., & Sohel, M. S. I. (2021). Agricultural drought
711 risk assessment of Northern New South Wales, Australia using geospatial
712 techniques. *Science of the Total Environment*, 756.
713 <https://doi.org/10.1016/j.scitotenv.2020.143600>
- 714 Huang, J. L., Qin, D. H., Jiang, T., Wang, Y. J., Feng, Z. Q., Zhai, J. Q., et al. (2019).
715 Effect of Fertility Policy Changes on the Population Structure and Economy of
716 China: From the Perspective of the Shared Socioeconomic Pathways. *Earths Future*,
717 7(3), 250–265. <https://doi.org/10.1029/2018ef000964>
- 718 IPCC. (2012). *Managing the risks of extreme events and disasters to advance climate*
719 *change adaptation: special report of the intergovernmental panel on climate change*
720 [Field, C.B., V. Barros, T.F. Stocker, D. Qin, D.J. Dokken, K.L. Ebi, M.D.
721 Mastrandrea, K.J. Mach, G.-K. Plattner, S.K. Allen, M. Tignor, and P.M. Midgley
722 (eds.)]. Cambridge, UK and New York, USA: Cambridge University Press.
- 723 IPCC. (2014). *Climate Change 2014: Synthesis Report. Contribution of Working Groups*
724 *I, II and III to the Fifth Assessment Report of the Intergovernmental Panel on Cli-*
725 *mate Change* [Core Writing Team, R.K. Pachauri and L.A. Meyer (eds.)]. Cam-

- 726 bridge, UK and New York, USA: Cambridge University Press.
- 727 IPCC. (2021). *Summary for Policymakers. In: Climate Change 2021: The Physical*
728 *Science Basis. Contribution of Working Group I to the Sixth Assessment Report of*
729 *the Intergovernmental Panel on Climate Change* [Masson-Delmotte, V., P. Zhai, A.
730 Pirani, S. L. Connors, C. Péan, S. Berger, N. Caud, Y. Chen, L. Goldfarb, M. I.
731 Gomis, M. Huang, K. Leitzell, E. Lonnoy, J.B.R. Matthews, T. K. Maycock, T.
732 Waterfield, O. Yelekçi, R. Yu and B. Zhou (eds.)]. Cambridge, UK and New York,
733 USA: Cambridge University Press. In Press.
- 734 ISFD Reduction. (2004). *Living with risk: a global review of disaster reduction initiatives.*
735 Geneva, CH: United Nations Publications.
- 736 Jiang, T., Zhao, J., Cao, L., Wang, Y., Su, B., Jing, C., et al. (2018). Projection of national
737 and provincial economy under the shared socioeconomic pathways in China.
738 *Progressus Inquisitiones de Mutatione Climatis*, 14(1), 50–58.
- 739 Jiang, T., Wang, Y., Yuan, J., Chen, Y., Gao, X., Jing, C., et al. (2018). Projection of
740 population and economy in the Belt and Road countries (2020-2060). *Progressus*
741 *Inquisitiones de Mutatione Climatis*, 14(2), 155–164.
- 742 Jing, C., Tao, H., Jiang, T., Wang, Y. J., Zhai, J. Q., Cao, L. G., & Su, B. D. (2020).
743 Population, urbanization and economic scenarios over the Belt and Road region
744 under the Shared Socioeconomic Pathways. *Journal of Geographical Sciences*,
745 30(1), 68–84. <https://doi.org/10.1007/s11442-020-1715-x>
- 746 Khoshnazar, A., Perez, G. A. C., & Diaz, V. (2021). Spatiotemporal Drought Risk
747 Assessment Considering Resilience and Heterogeneous Vulnerability Factors:
748 Lempa Transboundary River Basin in The Central American Dry Corridor. *Journal*
749 *of Marine Science and Engineering*, 9(4). <https://doi.org/10.3390/jmse9040386>
- 750 Kim, J. S., Park, S. Y., Hong, H. P., Chen, J., Choi, S. J., Kim, T. W., & Lee, J. H. (2020).
751 Drought risk assessment for future climate projections in the Nakdong River Basin,
752 Korea. *International Journal of Climatology*, 40(10), 4528–4540.
753 <https://doi.org/10.1002/joc.6473>
- 754 Kummu, M., Taka, M., & Guillaume, J. H. A. (2018). Data Descriptor: Gridded global
755 datasets for Gross Domestic Product and Human Development Index over
756 1990-2015. *Scientific Data*, 5. <https://doi.org/10.1038/sdata.2018.4>
- 757 Le, T., Sun, C., Choy, S., & Kuleshov, Y. (2021). Regional drought risk assessment in the
758 Central Highlands and the South of Vietnam. *Geomatics Natural Hazards & Risk*,
759 12(1), 3140–3159. <https://doi.org/10.1080/19475705.2021.1998232>

- 760 Lehner, F., Coats, S., Stocker, T. F., Pendergrass, A. G., Sanderson, B. M., Raible, C. C.,
761 & Smerdon, J. E. (2017). Projected drought risk in 1.5 degrees C and 2 degrees C
762 warmer climates. *Geophysical Research Letters*, *44*(14), 7419–7428.
763 <https://doi.org/10.1002/2017gl074117>
- 764 Lesk, C., Rowhani, P., & Ramankutty, N. (2016). Influence of extreme weather disasters
765 on global crop production. *Nature*, *529*(7584), 84-+.
766 <https://doi.org/10.1038/nature16467>
- 767 Li, H. W., Li, Z., Chen, Y. N., Xiang, Y. Y., Liu, Y. C., Kayumba, P. M., & Li, X. Y.
768 (2021). Drylands face potential threat of robust drought in the CMIP6 SSPs
769 scenarios. *Environmental Research Letters*, *16*(11).
770 <https://doi.org/10.1088/1748-9326/ac2bce>
- 771 Liu, X., Guo, P., Tan, Q., Zhang, F., Huang, Y., & Wang, Y. Z. (2021). Drought disaster
772 risk management based on optimal allocation of water resources. *Natural Hazards*,
773 *108*(1), 285–308. <https://doi.org/10.1007/s11069-021-04680-2>
- 774 Liu, Y. J., & Chen, J. (2021). Future global socioeconomic risk to droughts based on
775 estimates of hazard, exposure, and vulnerability in a changing climate. *Science of the*
776 *Total Environment*, *751*. <https://doi.org/10.1016/j.scitotenv.2020.142159>
- 777 Lloyd, C. T., Chamberlain, H., Kerr, D., Yetman, G., Pistolesi, L., Stevens, F. R., et al.
778 (2019). Global spatio-temporally harmonised datasets for producing high-resolution
779 gridded population distribution datasets. *Big Earth Data*, *3*(2), 108–139.
780 <https://doi.org/10.1080/20964471.2019.1625151>
- 781 Lu, Y. J., Cai, H. J., Jiang, T. T., Sun, S. K., Wang, Y. B., Zhao, J. F., et al. (2019).
782 Assessment of global drought propensity and its impacts on agricultural water use in
783 future climate scenarios. *Agricultural and Forest Meteorology*, *278*.
784 <https://doi.org/10.1016/j.agrformet.2019.107623>
- 785 Marengo, J. A., Torres, R. R., & Alves, L. M. (2017). Drought in Northeast Brazil-past,
786 present, and future. *Theoretical and Applied Climatology*, *129*(3–4), 1189–1200.
787 <https://doi.org/10.1007/s00704-016-1840-8>
- 788 McKee, T. B., Doesken, N. J., & Kleist, J. (1993). The relationship of drought frequency
789 and duration to time scales. In *Proceedings of the 8th Conference on Applied*
790 *Climatology* (Vol. 17, pp. 179–183). Boston.
- 791 Meijer, J. R., Huijbregts, M. A. J., Schotten, K., & Schipper, A. M. (2018). Global
792 patterns of current and future road infrastructure. *Environmental Research Letters*,
793 *13*(6). <https://doi.org/10.1088/1748-9326/aabd42>

- 794 Meza, I., Siebert, S., Doll, P., Kusche, J., Herbert, C., Rezaei, E. E., et al. (2020).
795 Global-scale drought risk assessment for agricultural systems. *Natural Hazards and*
796 *Earth System Sciences*, 20(2), 695–712. <https://doi.org/10.5194/nhess-20-695-2020>
- 797 Mokarram, M., Pourghasemi, H. R., Hu, M., & Zhang, H. C. (2021). Determining and
798 forecasting drought susceptibility in southwestern Iran using multi-criteria
799 decision-making (MCDM) coupled with CA-Markov model. *Science of the Total*
800 *Environment*, 781. <https://doi.org/10.1016/j.scitotenv.2021.146703>
- 801 Mondal, S. K., Huang, J. L., Wang, Y. J., Su, B. D., Zhai, J. Q., Tao, H., et al. (2021).
802 Doubling of the population exposed to drought over South Asia: CMIP6
803 multi-model-based analysis. *Science of the Total Environment*, 771.
804 <https://doi.org/10.1016/j.scitotenv.2021.145186>
- 805 Monerie, P. A., Wainwright, C. M., Sidibe, M., & Akinsanola, A. A. (2020). Model
806 uncertainties in climate change impacts on Sahel precipitation in ensembles of
807 CMIP5 and CMIP6 simulations. *Climate Dynamics*, 55(5–6), 1385–1401.
808 <https://doi.org/10.1007/s00382-020-05332-0>
- 809 Naumann, G., Alfieri, L., Wyser, K., Mentaschi, L., Betts, R. A., Carrao, H., et al. (2018).
810 Global Changes in Drought Conditions Under Different Levels of Warming.
811 *Geophysical Research Letters*, 45(7), 3285–3296.
812 <https://doi.org/10.1002/2017gl076521>
- 813 O'Neill, B. C., Tebaldi, C., van Vuuren, D. P., Eyring, V., Friedlingstein, P., Hurtt, G., et
814 al. (2016). The Scenario Model Intercomparison Project (ScenarioMIP) for CMIP6.
815 *Geoscientific Model Development*, 9(9), 3461–3482.
816 <https://doi.org/10.5194/gmd-9-3461-2016>
- 817 OECD. (2008). *Handbook on constructing composite indicators: methodology and user*
818 *guide*. Paris, FR: OECD publishing.
- 819 Palchauthuri, M., & Biswas, S. (2016). Application of AHP with GIS in drought risk
820 assessment for Puruliya district, India. *Natural Hazards*, 84(3), 1905–1920.
821 <https://doi.org/10.1007/s11069-016-2526-3>
- 822 Palmer, W. C. (1965). *Meteorological drought* (Vol. 30). Washington, DC: US
823 Department of Commerce, Weather Bureau.
- 824 Pearson, L., & Pelling, M. (2015). The UN Sendai framework for disaster risk reduction
825 2015–2030: Negotiation process and prospects for science and practice. *Journal of*
826 *Extreme Events*, 2(01), 1571001.
- 827 Peduzzi, P., Dao, H., Herold, C., & Mouton, F. (2009). Assessing global exposure and

- 828 vulnerability towards natural hazards: the Disaster Risk Index. *Natural Hazards and*
829 *Earth System Sciences*, 9(4), 1149–1159.
830 <https://doi.org/10.5194/nhess-9-1149-2009>
- 831 Prabnakorn, S., Maskey, S., Suryadi, F. X., & de Fraiture, C. (2019). Assessment of
832 drought hazard, exposure, vulnerability, and risk for rice cultivation in the Mun
833 River Basin in Thailand. *Natural Hazards*, 97(2), 891–911.
834 <https://doi.org/10.1007/s11069-019-03681-6>
- 835 Riahi, K., van Vuuren, D. P., Kriegler, E., Edmonds, J., O'Neill, B. C., Fujimori, S., et al.
836 (2017). The Shared Socioeconomic Pathways and their energy, land use, and
837 greenhouse gas emissions implications: An overview. *Global Environmental*
838 *Change-Human and Policy Dimensions*, 42, 153–168.
839 <https://doi.org/10.1016/j.gloenvcha.2016.05.009>
- 840 Saaty, T. L., & Vargas, L. G. (2001). Models, methods, concepts & applications of the
841 analytic hierarchy process. *International Series in Operations Research and*
842 *Management Science*. <https://doi.org/10.1007/978-1-4615-1665-1>
- 843 Saaty, T. L. (1987). Rank generation, preservation, and reversal in the analytic hierarchy
844 decision process. *Decision Sciences*, 18(2), 157–177.
845 <https://doi.org/10.1111/j.1540-5915.1987.tb01514.x>
- 846 Sahana, V., Mondal, A., & Sreekumar, P. (2021). Drought vulnerability and risk
847 assessment in India: Sensitivity analysis and comparison of aggregation techniques.
848 *Journal of Environmental Management*, 299.
849 <https://doi.org/10.1016/j.jenvman.2021.113689>
- 850 Sian, K., Wang, J. H., Ayugi, B. O., Nooni, I. K., & Ongoma, V. (2021). Multi-Decadal
851 Variability and Future Changes in Precipitation over Southern Africa. *Atmosphere*,
852 12(6). <https://doi.org/10.3390/atmos12060742>
- 853 Song, Y. L., Tian, J. F., Linderholm, H. W., Wang, C. Y., Ou, Z. R., & Chen, D. L. (2021).
854 The contributions of climate change and production area expansion to drought risk
855 for maize in China over the last four decades. *International Journal of Climatology*,
856 41, E2851–E2862. <https://doi.org/10.1002/joc.6885>
- 857 Spinoni, J., Naumann, G., Carrao, H., Barbosa, P., & Vogt, J. (2014). World drought
858 frequency, duration, and severity for 1951-2010. *International Journal of*
859 *Climatology*, 34(8), 2792–2804. <https://doi.org/10.1002/joc.3875>
- 860 Spinoni, J., Vogt, J. V., Naumann, G., Barbosa, P., & Dosio, A. (2018). Will drought
861 events become more frequent and severe in Europe? *International Journal of*

- 862 *Climatology*, 38(4), 1718–1736. <https://doi.org/10.1002/joc.5291>
- 863 Su, B. D., Huang, J. L., Fischer, T., Wang, Y. J., Kundzewicz, Z. W., Zhai, J. Q., et al.
864 (2018). Drought losses in China might double between the 1.5 degrees C and 2.0
865 degrees C warming. *Proceedings of the National Academy of Sciences of the United*
866 *States of America*, 115(42), 10600–10605.
867 <https://doi.org/10.1073/pnas.1802129115>
- 868 Su, B. D., Huang, J. L., Mondal, S. K., Zhai, J. Q., Wang, Y. J., Wen, S. S., et al. (2021).
869 Insight from CMIP6 SSP-RCP scenarios for future drought characteristics in China.
870 *Atmospheric Research*, 250. <https://doi.org/10.1016/j.atmosres.2020.105375>
- 871 Sun, Z. Y., Zhang, J. Q., Zhang, Q., Hu, Y., Yan, D. H., & Wang, C. Y. (2014). Integrated
872 risk zoning of drought and waterlogging disasters based on fuzzy comprehensive
873 evaluation in Anhui Province, China. *Natural Hazards*, 71(3), 1639–1657.
874 <https://doi.org/10.1007/s11069-013-0971-9>
- 875 Tabari, H., Hosseinzadehtalaei, P., AghaKouchak, A., & Willems, P. (2019). Latitudinal
876 heterogeneity and hotspots of uncertainty in projected extreme precipitation.
877 *Environmental Research Letters*, 14(12). <https://doi.org/10.1088/1748-9326/ab55fd>
- 878 Takeshima, A., Kim, H., Shiogama, H., Lierhammer, L., Scinocca, J. F., Seland, O., &
879 Mitchell, D. (2020). Global aridity changes due to differences in surface energy and
880 water balance between 1.5 degrees C and 2 degrees C warming. *Environmental*
881 *Research Letters*, 15(9). <https://doi.org/10.1088/1748-9326/ab9db3>
- 882 Tang, B., Hu, W. T., & Duan, A. M. (2021). Assessment of Extreme Precipitation Indices
883 over Indochina and South China in CMIP6 Models. *Journal of Climate*, 34(18),
884 7507–7524. <https://doi.org/10.1175/jcli-d-20-0948.1>
- 885 Thilakarathne, M., & Sridhar, V. (2017). Characterization of future drought conditions in
886 the Lower Mekong River Basin. *Weather and Climate Extremes*, 17, 47–58.
887 <https://doi.org/10.1016/j.wace.2017.07.004>
- 888 Touma, D., Ashfaq, M., Nayak, M. A., Kao, S. C., & Diffenbaugh, N. S. (2015). A
889 multi-model and multi-index evaluation of drought characteristics in the 21st
890 century. *Journal of Hydrology*, 526, 196–207.
891 <https://doi.org/10.1016/j.jhydrol.2014.12.011>
- 892 Ukkola, A. M., De Kauwe, M. G., Roderick, M. L., Abramowitz, G., & Pitman, A. J.
893 (2020). Robust Future Changes in Meteorological Drought in CMIP6 Projections
894 Despite Uncertainty in Precipitation. *Geophysical Research Letters*, 47(11).
895 <https://doi.org/10.1029/2020gl087820>

- 896 Vicente-Serrano, S. M., Begueria, S., & Lopez-Moreno, J. I. (2010). A Multiscalar
897 Drought Index Sensitive to Global Warming: The Standardized Precipitation
898 Evapotranspiration Index. *Journal of Climate*, 23(7), 1696–1718.
899 <https://doi.org/10.1175/2009jcli2909.1>
- 900 Vicente-Serrano, S. M., Quiring, S. M., Pena-Gallardo, M., Yuan, S. S., &
901 Dominguez-Castro, F. (2020). A review of environmental droughts: Increased risk
902 under global warming? *Earth-Science Reviews*, 201.
903 <https://doi.org/10.1016/j.earscirev.2019.102953>
- 904 van Vuuren, D. P., Kriegler, E., O'Neill, B. C., Ebi, K. L., Riahi, K., Carter, T. R., et al.
905 (2014). A new scenario framework for Climate Change Research: scenario matrix
906 architecture. *Climatic Change*, 122(3), 373–386.
907 <https://doi.org/10.1007/s10584-013-0906-1>
- 908 Wang, T., Tu, X. J., Singh, V. P., Chen, X. H., & Lin, K. R. (2021). Global data
909 assessment and analysis of drought characteristics based on CMIP6. *Journal of*
910 *Hydrology*, 596. <https://doi.org/10.1016/j.jhydrol.2021.126091>
- 911 WMO. (2021). *WMO Atlas of Mortality and Economic Losses from Weather, Climate*
912 *and Water Extremes (1970–2019)*. Geneva, CH: World Meteorological
913 Organization.
- 914 Yan, D. H., Wang, K., Qin, T. L., Weng, B. S., Wang, H., Bi, W. X., et al. (2019). A data
915 set of global river networks and corresponding water resources zones divisions
916 (Version 6) [Dataset]. Figshare. <https://doi.org/10.6084/m9.figshare.8044184.v6>
- 917 Yao, J. Q., Zhao, Y., Chen, Y. N., Yu, X. J., & Zhang, R. B. (2018). Multi-scale
918 assessments of droughts: A case study in Xinjiang, China. *Science of the Total*
919 *Environment*, 630, 444–452. <https://doi.org/10.1016/j.scitotenv.2018.02.200>
- 920 Yin, Q., Wang, J. F., Ren, Z. P., Li, J., & Guo, Y. M. (2019). Mapping the increased
921 minimum mortality temperatures in the context of global climate change. *Nature*
922 *Communications*, 10. <https://doi.org/10.1038/s41467-019-12663-y>
- 923 Yin, Y. Y., Gao, Y., Lin, D. G., Wang, L., Ma, W. D., & Wang, J. A. (2021). Mapping the
924 Global-Scale Maize Drought Risk Under Climate Change Based on the
925 GEPIC-Vulnerability-Risk Model. *International Journal of Disaster Risk Science*,
926 12(3), 428–442. <https://doi.org/10.1007/s13753-021-00349-3>
- 927 Yue, T. X., Fan, Z. M., & Liu, J. Y. (2005). Changes of major terrestrial ecosystems in
928 China since 1960. *Global and Planetary Change*, 48(4), 287–302.
929 <https://doi.org/10.1016/j.gloplacha.2005.03.001>

- 930 Yue, T. X., Fan, Z. M., Liu, J. Y., & Wei, B. X. (2006). Scenarios of major terrestrial
931 ecosystems in China. *Ecological Modelling*, *199*(3), 363–376.
932 <https://doi.org/10.1016/j.ecolmodel.2006.05.026>
- 933 Yue, T. X., Fan, Z. M., & Liu, J. Y. (2007). Scenarios of land cover in China. *Global and*
934 *Planetary Change*, *55*(4), 317–342. <https://doi.org/10.1016/j.gloplacha.2006.10.002>
- 935 Zhang, Q., Yao, Y. B., Wang, Y., Wang, S. P., Wang, J. S., Yang, J. H., et al. (2019).
936 Characteristics of drought in Southern China under climatic warming, the risk, and
937 countermeasures for prevention and control. *Theoretical and Applied Climatology*,
938 *136*(3–4), 1157–1173. <https://doi.org/10.1007/s00704-018-2541-2>
- 939 Zhang, X., Wei, C. H., Obringer, R., Li, D. R., Chen, N. C., & Niyogi, D. (2017). Gauging
940 the Severity of the 2012 Midwestern US Drought for Agriculture. *Remote Sensing*,
941 *9*(8). <https://doi.org/10.3390/rs9080767>
- 942 Zheng, H. X., Chiew, F. H. S., Charles, S., & Podger, G. (2018). Future climate and
943 runoff projections across South Asia from CMIP5 global climate models and
944 hydrological modelling. *Journal of Hydrology-Regional Studies*, *18*, 92–109.
945 <https://doi.org/10.1016/j.ejrh.2018.06.004>